Controlled quantum dot array segmentation via highly tunable interdot tunnel coupling

Martin Nurizzo, Baptiste Jadot, Pierre-André Mortemousque, Vivien Thiney, Emmanuel Chanrion, Matthieu Dartiailh, Arne Ludwig, Andreas D. Wieck, Christopher Bäuerle, Matias Imanol Urdampilleta, et al.

Applied Physics Letters ARTICLE scitation.org/journal/apl

Controlled quantum dot array segmentation via highly tunable interdot tunnel coupling

Cite as: Appl. Phys. Lett. **121**, 084001 (2022); doi: 10.1063/5.0105635
Submitted: 24 June 2022 · Accepted: 28 July 2022 ·
Published Online: 22 August 2022

Martin Nurizzo,[1,a)] Baptiste Jadot,[2] Pierre-André Mortemousque,[2] Vivien Thiney,[2] Emmanuel Chanrion,[1] Matthieu Dartiailh,[1] Arne Ludwig,[3] Andreas D. Wieck,[3] Christopher Bäuerle,[1] Matias Urdampilleta,[1] and Tristan Meunier[1,b)]

AFFILIATIONS

[1]University Grenoble Alpes, CNRS, Grenoble INP, Institut Néel, F-38000 Grenoble, France
[2]University Grenoble Alpes, CEA, Leti, F-38000 Grenoble, France
[3]Lehrstuhl für Angewandte Festkörperphysik, Ruhr-Universität Bochum, Universitätsstraße 150, D-44780 Bochum, Germany

[a)]Author to whom correspondence should be addressed: martin.nurizzo@neel.cnrs.fr
[b)]Electronic mail: tristan.meunier@neel.cnrs.fr

ABSTRACT

Recent demonstrations using electron spins stored in quantum dot array as qubits are promising for developing a scalable quantum computing platform. An ongoing effort is, therefore, aiming at the precise control of the quantum dot parameters in larger and larger arrays which represents a complex challenge. Partitioning of the system with the help of the inter-dot tunnel barriers can lead to a simplification for tuning and offers a protection against unwanted charge displacement. In a triple quantum dot system, we demonstrate a nanosecond control of the inter-dot tunnel rate permitting to reach the two extreme regimes, large GHz tunnel coupling, and sub-Hz isolation between adjacent dots. We use this development to isolate a subpart of the array in a metastable configuration while performing charge displacement and readout in the rest of the system. The degree of control over tunnel coupling achieved in a unit cell should motivate future protocol development for tuning, manipulation, and readout including this capability.

Arrays of quantum dots (QDs) are identified as one possible road for scaling up electron spin-based quantum processors.[1–4] In this context, the ability to displace controllably individual electrons plays an important role for realizing elementary operations within the array. Displacement at the QD scale induces coherent manipulation and interaction,[5–8] while shuttling of the electrons at multi-dot scale enables array filling[9,10] and functionalities for long distance quantum interconnection.[9,11,12] These capabilities come with potential sources of errors such as incorrect positioning and tunneling while operating the electron spin qubits. It is, therefore, desirable to find protocols to minimize their impact on the rest of the qubits. Recent demonstrations of highly tunable interdot tunnel coupling[9,13,14] could offer strategies to protect the electron spin information while enabling quantum manipulation capabilities. In semiconductor devices, this method is commonly used to isolate QD arrays from electron reservoirs, thereby fixing the total number of charges in the system.[14,15]

Here, we characterize the inter-dot tunnel rate from the sub-Hz to GHz regime via the study of metastable charge states and achieve complete isolation both from the reservoirs and the neighbor QD of up to three electrons. Then, we implement two functionalities demonstrating the potential of the array partitioning process. First, an improvement in metastable charge state lifetime and its readout at a fixed and optimized position, and then charge displacement and readout in the partitioned array.

The device measured in this work is presented in Fig. 1(a) and is composed of a linear triple QD array defined electrostatically by voltages applied to metallic gates on a GaAs/AlGaAs heterostructure. The electrometer consists of a single electron transistor (SET) set on the side of a Coulomb peak to be sensitive to the charge configuration of the array. The QD array is tuned by adjusting the voltage applied on the gates labeled as B_{1-4}. The gate voltages applied for each experiment discussed are summarized in Sec. I of the supplementary material. We first focus on the protocol to isolate a quantum dot from the reservoirs. The first step is to load electrons from the bottom left reservoir [Fig. 1(a)] to the previously emptied QD nanostructure. We show in Fig. 1(b) a so-called stability diagram where we vary the voltages applied on B_1 and B_2 while recording the current i_{SET} through the electrometer. In this diagram, it is possible to determine the absolute

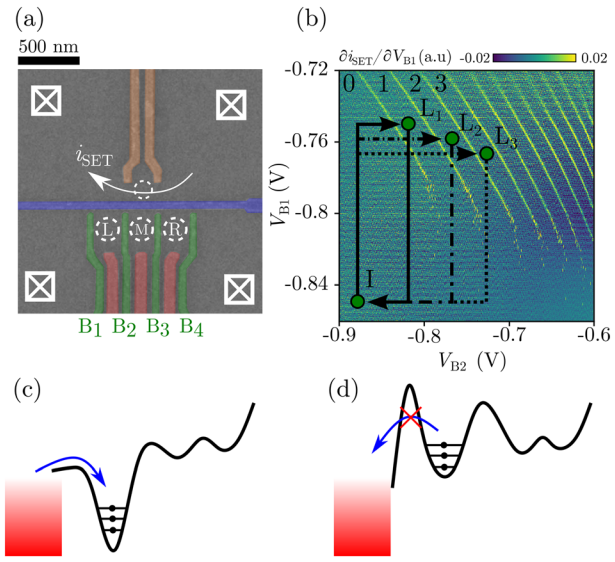

FIG. 1. Device, electron loading, and isolation from the reservoirs. (a) Electron micrograph of a sample similar to the measured one. (b) Stability diagram of the leftmost QD. The derivative of the current (with respect to V_{B1}) measured across the SET is plotted as a function of the voltage applied on B_1 and B_2 gates controlling the reservoir-QD tunnel barrier height and the chemical potential of the QD, respectively. The electron occupation number is indicated for the first four charge regions of the stability diagram. The indicated positions such as L_1, L_2, L_3, and I are used to load one, two, and three electrons in the left QD and to isolate the QD array from the left electron reservoir, respectively. (c) Schematic of the potential landscape at position L_3 of the stability diagram. (d) Schematic of the potential landscape at position I of the stability diagram after the loading procedure.

number of electrons in the dot by identifying regions separated by charge degeneracy lines. The chemical potential of QD L is controlled by the voltage applied on B_2, while the reservoir to QD tunnel coupling is controlled by the voltage applied to B_1, as indicated by the disappearance of the charge degeneracy lines for $V_{B1} < -0.8$ V. The interruption of the degeneracy lines is an indicator of the isolated regime where the electron exchange rate with the reservoir is slower than the measurement sweep rate (250 mV s^{-1}). We engineered a pulse sequence to load the desired number of electrons in the QD structure and isolate them from the reservoir. The system is first initialized at point I empty of any electrons and the pulse sequence drawn on top of the stability diagram of Fig. 1(b) is applied. A voltage pulse on B_1 gate increases coupling between the array and the reservoir, allowing the exchange of electrons with dot L. Then, the chemical potential of the left QD is lowered by applying a voltage pulse on gate B_2. By varying the amplitude of this pulse to reach either the point L_1, L_2, or L_3, it is possible to load one, two, or three electrons in the dot, respectively. A sketch of the potential landscape at the position L_3 is pictured in Fig. 1(c). From the selected position, voltage pulses are applied on gate B_1 and then B_2 to reach the position I, where the electron tunneling to the reservoir is suppressed (see Sec. II of the supplementary material). In this configuration, the high chemical potential of the left QD guarantees that all loaded electrons should eventually tunnel back to the reservoir leaving the QD empty. However, due to low tunnel coupling to the reservoir, this metastable configuration can be held for several tens of seconds (see Sec. II of the supplementary material).

In this section, the isolation process is pushed one step further to perform array partitioning by demonstrating QD-to-QD decoupling. We note the charge configuration of the array (l, m, r) with l, m, and r being the charge occupation of the QDs L, M, and R, respectively. After loading either one, two, or three electrons in L, we vary the voltages applied on B_2 and B_3 to progressively transfer charges to dot M. The corresponding stability diagrams are presented in Figs. 2(c)–2(e). For a system of n dots containing a total of k electrons, we expect $\binom{n+k-1}{k}$ charge states, which we experimentally observe for $n = 2$ and k up to 3. Analogous to QD-reservoir decoupling, we observe the apparition of stochastic events as V_{B2} becomes

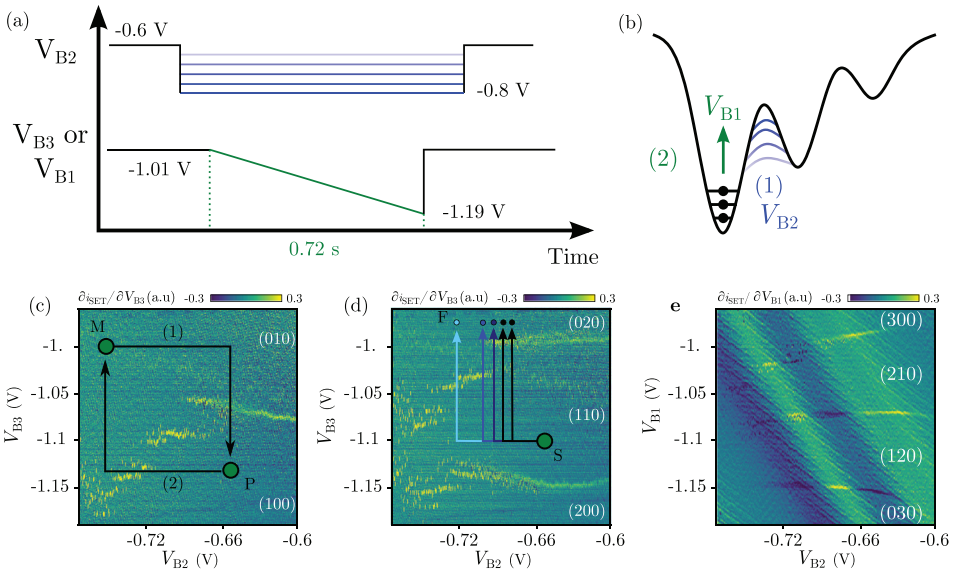

FIG. 2. One, two, and three electrons stability diagram of a DQD. (a) Chronograph of the voltages applied to $V_{B1/3}$ and V_{B2} to perform the stability diagram (c)–(e). (b) Schematic of the potential landscape of the QD array during the stability diagram (e). (c)–(e) Stability diagram of the L–M DQD performed with a fixed number of charges one, two, and three isolated from the reservoirs, respectively. The detuning and the tunnel coupling of the L–M DQD are swept using the relevant gates B_3 and B_2. It is possible to access all charge states of the DQD by sweeping B_3 or B_1 gate voltage over around 200 mV. For a negative enough voltage applied on B_2, the stability diagram exhibits excited charge states of the DQD that are only observable in the low tunnel coupling regime. Charge configurations of the array are indicated in white.

increasingly more negative. This phenomenon now corresponds to the L–M inter-dot tunnel rate becoming comparable to the measurement sweep rate (250 mV s^{-1}).

In order to quantify the metastable charge state relaxation rate dependence with the voltage applied on gate B_2, we designed the pulse sequence sketched on top of the stability diagrams in Fig. 2(d). Two electrons are loaded in L and the system is brought in the (110) configuration at position S. From this point, the interdot tunnel rate is lowered to the desired value V_{B2}^{F} using a voltage pulse on the gate B_2. After 100 ns, the detuning is set to reach the (020) charge region via a voltage pulse on gate B_3. At this position, the (110) charge state becomes metastable. To track the evolution of the charge state, we record the current i_{SET} during up to 1 s. The procedure is repeated 1000 times for V_{B2}^{F} between −0.72 and −0.68 V. Selected records of i_{SET} for $V_{B2}^{F} = -0.69$ V are shown in Fig. 3(b) and we observe sharp single jumps of i_{SET} from 0.55 to 0.75 nA. These events are associated with an electron tunneling from M to L. In Fig. 3(c), we compute the probability $P_{(110)}$ to observe the (110) charge state as a function of the waiting time at point F and observe an exponential decay of the population. In Fig. 3(d), we observe that the charge state lifetime can be tuned over 4 orders of magnitude in few tens of mV. In particular, for $V_{B2}^{F} \leqslant -0.72$ V, no relaxation events are visible in a thousand 1 s-long time-traces, setting a higher relaxation rate bound at 10^{-2} Hz. This demonstrates that we are able to reduce the inter-dot relaxation rate well below the Hz regime while keeping the initial QD structure intact. Moreover, the high level of control in the low inter-dot tunnel coupling regime did not prevent us to perform spin qubit operations which requires GHz tunnel coupling in the same sample with the same tuning (data not shown here).

As the capability to operate over such a wide range, inter-dot tunnel coupling enables functionalities for future prospects in spin qubit technology.[2] Indeed, freezing on a fast timescale, the electron dynamics results in a well separated and metastable charge configuration that can be efficiently probed. Proof of principle experiment is performed in a tunnel coupled double quantum dot (DQD) with up to three electrons. The protocol consists of loading a specific charge configuration in the double dot, decreasing the fast timescale of the tunnel barrier, and then tuning the system to a working point at which the charge detection has been optimized while preserving the charge configuration.

To do so, we manipulate inter-dot tunnel coupling and the detuning of the L–M DQD at the nanosecond timescale. The initialization of the metastable charge configuration of the array is characterized using a freeze map protocol. It consists of setting the system at a given detuning and tunnel coupling value before pulsing the inter-dot tunnel rate to the sub-Hz regime to freeze the charge configuration. Followed by a charge readout, this protocol allows us to identify the detuning and tunnel coupling regions where a charge transfer is possible.

In addition to the already described notation for labeling the charge states, we introduce a vertical bar | indicating a sub-Hz tunnel coupling rate in between the QDs. The trajectory, visible in Fig. 2(c), starts in the (0|10) charge state at point M and is used to realize the freeze map protocol. Two 100 ns voltages pulses applied sequentially to B_2 and B_3 set the system to point P. Then, the inter-dot tunnel rate is lowered to the sub-Hz regime and the detuning is set back to position M. At this position, the electrometer signal i_{SET} is averaged during 5 ms. Depending on the coordinates of point P (V_{B2}^{P}, V_{B3}^{P}), we obtain

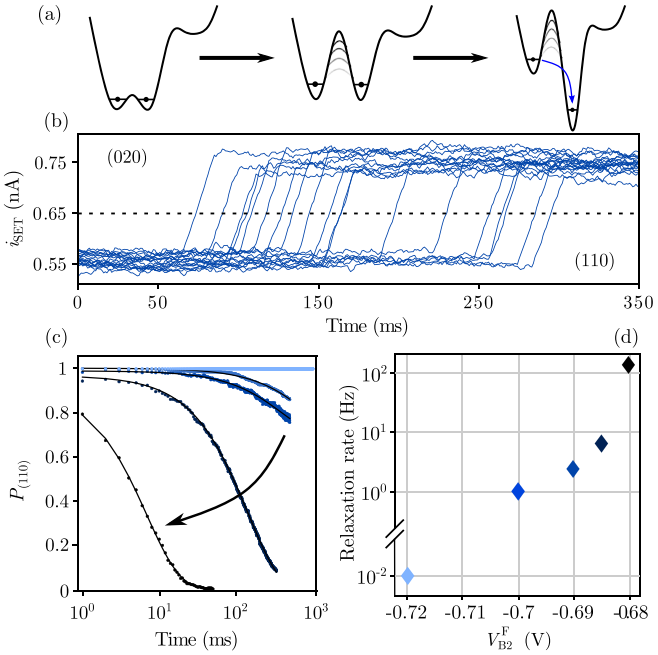

FIG. 3. Probing relaxation process of a metastable charge state in DQD. (a) Schematic of the potential landscape during the relaxation procedure. The system is initialized to point P in the (110) charge configuration. The tunnel barrier height between the dots is set by applying a pulse of varying amplitude V_{B2}^{F}. The system is then brought back in the region where the equilibrium charge state of the array is (020). (b) Selected single shot measurements of (110) to (020) relaxation for $V_{B2}^{F} = -0.69$ V. The current i_{SET} displays single event relaxation. A moving average filter is applied to the traces for clarity. (c) Relaxation of the (110) to (020) charge state observed for different tunnel barrier heights. A threshold is defined halfway between the two current levels represented by a dashed line in (a). For the 1000 traces, a current above or below this threshold is associated with (110) or (020) charge state, respectively. The binarized traces are averaged for each V_{B2}^{F} value tested to compute the (110) population. Experimental data are represented as solid points and the solid black line is an exponential decay fit. For $V_{B2}^{F} = -0.72$ V, we do not observe any relaxation event in 1000 shots of 1 s. (d) Relaxation rate of the (110) to the (020) charge state as a function of the freeze point (F) coordinate.

two possible values for i_{SET} corresponding to either the (0|10) or (1|00) charge state, as shown in Fig. 4(b). Comparing with the stability diagram in Fig. 2(c), for $V_{B2} > -0.65$ V, we observe the same charge transition at $V_{B3} = -1.07$ V. It indicates that the time spent at P is sufficient to observe charge transfer. For $V_{B2} < -0.65$ V, the tunnel coupling rate is not strong enough to allow charge transfer in the ground state at $V_{B3} = -1.07$ V. Nevertheless, by increasing the detuning ($V_{B3} < -1.07$ V), higher orbital states of M with higher tunnel coupling are accessible and allow the charge transfer within the time spent in P. The complete description of the charge dynamics to account for the precise shape of the charge transition is beyond the scope of this work and will be studied further in subsequent experiments. As shown in Figs. 4(c) and 4(d), the agreement between the freeze map and the stability diagram is also observed for two and three electrons loaded in the array considering that B_1 and B_3 have an opposite but similar effect on the potential detuning of the L–M DQD. To conclude, we demonstrated the capability to initialize metastable

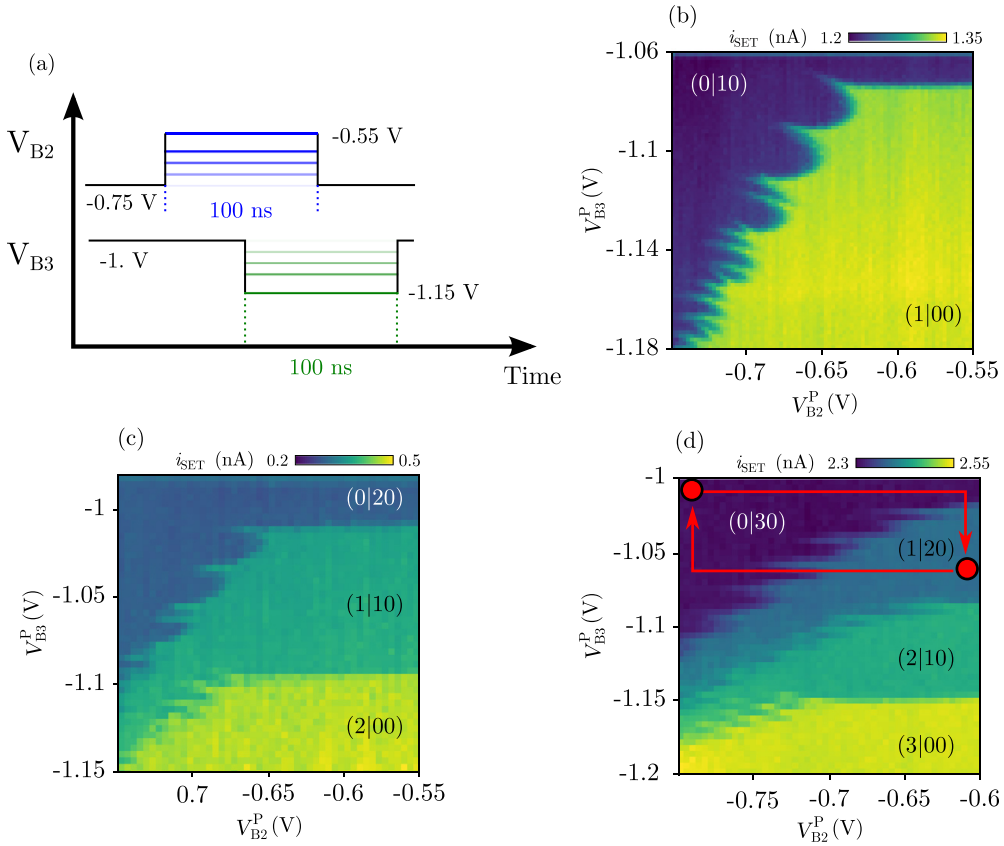

FIG. 4. One, two, and three electrons freeze map in a DQD. (a) Chronograph of the voltages applied to gates B_3 and B_2 to perform the freeze map in (b). (b)–(d) One, two, and three electrons freeze map of the L–M DQD. The measurements are obtained by performing the pulse sequence sketched on top of the stability diagram in Fig. 2(c). The first pulse probes the DQD at a certain value of detuning and tunnel coupling at a varied point P. The second one brings back the system at point M by first setting the tunnel coupling in the sub-Hz regime and then the detuning. Finally, the current i_{SET} is recorded during 5 ms. Each pixel is the average of 50 realizations of the freeze map protocol. For $V_{B2} > -0.6$ V, the electrons are transferred faster than 100 ns, approaching the regime of GHz coupling.

charge configurations for a duration long enough to permit their readout at an optimized position in the voltage gate space. This study is a demonstration of the initialization and readout protocols induced by the high level of control over inter-dot tunnel coupling.

In addition to an improvement of the charge determination in QD arrays, the inter-dot tunnel coupling control also grants us the possibility to isolate subparts of a QD array to simplify the tuning and manipulation. In this section, we demonstrate the complete isolation of a subpart of the QD array while keeping the complete control over the charge configuration in the rest of the system. To do so, we initialize a metastable charge state of the L–M DQD in order to isolate an electron in L. Then, we progressively transfer the charges remaining in M to R to control the number of electrons present in the M–R DQD subsystem.

The first step to implement this protocol consists of loading three electrons in M to reach the (030) charge state. From there, a (1|20) metastable charge configuration is initialized by pulsing the voltages applied on gates B_2 and B_3, an equivalent of the pulse sequence performed is sketched on top of the freeze map in Fig. 4(d). The next step consists in opening the tunneling between M and R by applying -0.65 V on gate B_3 and lowering the chemical potential of R closer to the one of M by increasing the voltage applied on B_4 to -1.15 V. In this voltage configuration, L–M inter-dot tunnel coupling is pulsed during 1 ms using a voltage pulse of amplitude V^T_{B2}. Following the pulse, the detuning of L–R is ramped using the voltage applied on gate B_4, while i_{SET} is recorded. The derivative $\partial i_{SET}/\partial V_{B4}$ is plotted as a function of V^R_{B4} and V^T_{B2} in Fig. 5(c). For $V^T_{B2} < -0.75$ V, we observe two degeneracy lines in the stability diagram indicating that the subarray composed of M and R QDs contains only two electrons, while the third one is isolated in L. Due to low L–M inter-dot tunnel coupling, the electron in L cannot tunnel back to M during the whole 1.2 s ramp; in this configuration, the only charge states available by the array are $(1|02)$, $(1|11)$, and $(1|02)$ (see Sec. III of the supplementary material). They are identified and labeled on top of the stability diagram. For a pulse amplitude $V^T_{B2} > -0.75$ V, we observe a third line, indicating that the electron stored in L tunneled back to M during the V^T_{B2} pulse. Indeed, this configuration allows the relaxation of the (120) to the (030) charge state and the resulting stability diagram corresponds to a classical one for three electrons loaded in a DQD. To conclude, we are able to perform electron manipulation in a partitioned DQD while preserving the charge state in the adjacent QD. This study demonstrates the ability of the array partitioning to lower

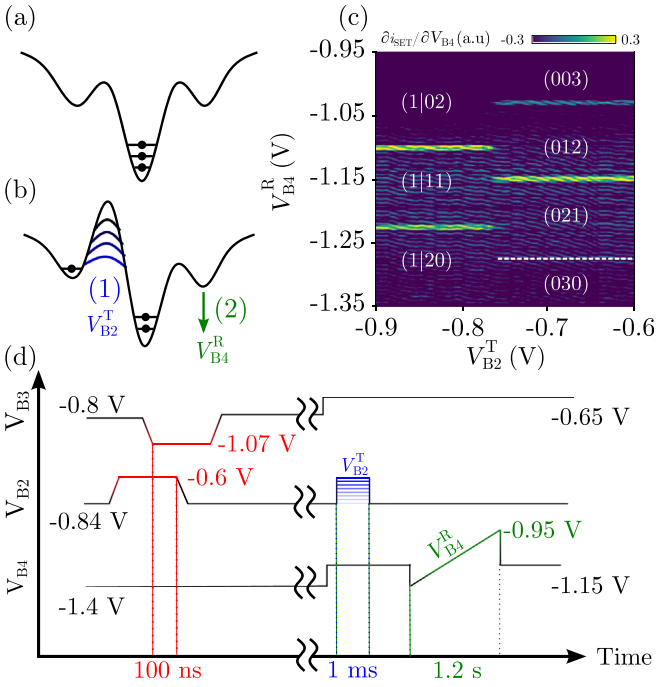

FIG. 5. Isolating subparts of the linear QD array. (a) Schematic of the potential landscape at the initialization point. (b) Schematic of the potential landscape at the beginning of the stability diagram of figure (c). (c) Stability diagram performed while a part of the array is segmented. For $V^T_{B2} < -0.75$ V, the electron in L is unable to tunnel back to M and the only charge state seen on the stability diagram are (1|20), (1|11), and (1|02). For higher values of V^T_{B2}, the electron in L tunnels back to M and all charge states of three electrons in a DQD are observed. (d) Chronograph of the voltages applied on gates B_2, B_3, and B_4. The pre-sequence is dedicated to create a metastable charge state (1|20) using the pulse sequence described in Fig. 4(d). Then, the voltage applied on the B_2 gate is pulsed during 1 ms to V^T_{B2} and finally the chemical potential of the R QD is ramped while the current i_{SET} is recorded.

the complexity of the stability diagrams by reducing the number of charge states available for the electrons.

The control of tunnel coupling and the chemical potential of each QD on fast timescales allowed us to initialize arbitrary metastable charge state of up to three electrons in a DQD. The freeze map protocol developed in this article allowed us to enhance the lifetime and perform readout of these states at a fixed and optimized position in the voltage gate space. This demonstration is of particular interest in the context of the wide use of Pauli spin blocked spin to charge conversion whose fidelity is limited by the lifetime of such metastable charge states.[16] We finally performed a segmentation of the array by decoupling a QD filled with one electron in a metastable configuration while performing charge displacement and readout in the rest of the structure. Doing so, we observed a reduction in the charge states available for the system, and therefore, a reduction in the complexity while tuning the QD array. The protocols developed in this Letter were using the particularities of metastable charge states; however, coupling our work to a precise study of the gate crosstalk and lever arm should allow us to easily perform a segmentation of the array while remaining in the charge ground state of the system. In this regime, the partitioning protocol opens the door to more complex applications such as the operation of larger 1D or 2D arrays of QDs while keeping the low dimensionality of simple subsystems.[17]

See the supplementary material for additional information of the array tuning and the array partitioning protocol.

We acknowledge the technical support from the Pole groups of the Institut Néel, and in particular, the NANOFAB team who helped with the sample realization, as well as T. Crozes, E. Eyraud, D. Lepoittevin, C. Hoarau, and C. Guttin. This work was supported by the ERC QUCUBE (Grant Agreement No. 810504). A.L. and A.D.W. gratefully acknowledge the support of Nos. DFG-TRR160 and DFH/UFA CDFA-05-06, DFG Project No. 383065199, and BMBF QR.X Project No. 16KISQ009.

AUTHOR DECLARATIONS

Conflict of Interest

The authors have no conflicts to disclose.

Author Contributions

Martin Nurizzo: Conceptualization (equal); Data curation (equal); Formal analysis (equal); Investigation (equal); Methodology (equal); Visualization (equal); Writing – original draft (equal); Writing – review and editing (equal). **Matias Urdampilleta:** Conceptualization (equal); Supervision (equal); Writing – review and editing (equal). **Tristan Meunier:** Conceptualization (equal); Formal analysis (equal); Funding acquisition (equal); Investigation (equal); Methodology (equal); Supervision (equal); Validation (equal); Visualization (equal); Writing – review and editing (equal). **Baptiste Jadot:** Conceptualization (equal); Data curation (equal); Formal analysis (equal); Methodology (equal); Supervision (equal); Writing – review and editing (equal). **Pierre-André Mortemousque:** Conceptualization (equal); Supervision (equal); Validation (equal); Writing – review and editing (equal). **Vivien Thiney:** Resources (equal); Supervision (equal); Writing – review and editing (supporting). **Emmanuel Chanrion:** Conceptualization (equal); Investigation (equal); Methodology (equal); Supervision (equal); Validation (equal); Writing – review and editing (supporting). **Matthieu C. Dartiailh:** Resources (equal); Supervision (equal); Writing – review and editing (equal). **Arne Ludwig:** Resources (equal); Writing – review and editing (supporting). **Andreas D. Wieck:** Resources (equal); Writing – review and editing (supporting). **Christopher Bauerle:** Resources (equal); Supervision (equal); Writing – review and editing (equal).

DATA AVAILABILITY

The data that support the findings of this study are available from the corresponding author upon reasonable request.

REFERENCES

[1]M. Vinet, L. Hutin, B. Bertrand, S. Barraud, J.-M. Hartmann, Y.-J. Kim, V. Mazzocchi, A. Amisse, H. Bohuslavskyi, L. Bourdet, A. Crippa, X. Jehl, R. Maurand, Y.-M. Niquet, M. Sanquer, B. Venitucci, B. Jadot, E. Chanrion, P.-A. Mortemousque, C. Spence, M. Urdampilleta, S. D. Franceschi, and T. Meunier, "Towards scalable silicon quantum computing," in *2018 IEEE International Electron Devices Meeting (IEDM)* (IEEE, 2018), pp. 6.5.1–6.5.4.

[2]R. Li, L. Petit, D. P. Franke, J. P. Dehollain, J. Helsen, M. Steudtner, N. K. Thomas, Z. R. Yoscovits, K. J. Singh, S. Wehner, L. M. K. Vandersypen, J. S.

Clarke, and M. Veldhorst, "A crossbar network for silicon quantum dot qubits," Sci. Adv. **4**, eaar3960 (2018).
[3]M. Veldhorst, H. G. J. Eenink, C. H. Yang, and A. S. Dzurak, "Silicon CMOS architecture for a spin-based quantum computer," Nat. Commun. **8**, 1766 (2017).
[4]L. M. K. Vandersypen, H. Bluhm, J. S. Clarke, A. S. Dzurak, R. Ishihara, A. Morello, D. J. Reilly, L. R. Schreiber, and M. Veldhorst, "Interfacing spin qubits in quantum dots and donors—hot, dense, and coherent," npj Quantum Inf. **3**, 34 (2017).
[5]J. R. Petta, A. C. Johnson, J. M. Taylor, E. A. Laird, A. Yacoby, M. D. Lukin, C. M. Marcus, M. P. Hanson, and A. C. Gossard, "Coherent manipulation of coupled electron spins in semiconductor quantum dots," Science **309**, 2180–2184 (2005).
[6]R. Brunner, Y.-S. Shin, T. Obata, M. Pioro-Ladrière, T. Kubo, K. Yoshida, T. Taniyama, Y. Tokura, and S. Tarucha, "Two-qubit gate of combined single-spin rotation and interdot spin exchange in a double quantum dot," Phys. Rev. Lett. **107**, 146801 (2011).
[7]T. F. Watson, S. G. J. Philips, E. Kawakami, D. R. Ward, P. Scarlino, M. Veldhorst, D. E. Savage, M. G. Lagally, M. Friesen, S. N. Coppersmith, M. A. Eriksson, and L. M. K. Vandersypen, "A programmable two-qubit quantum processor in silicon," Nature **555**, 633–637 (2018).
[8]J. Yoneda, K. Takeda, T. Otsuka, T. Nakajima, M. R. Delbecq, G. Allison, T. Honda, T. Kodera, S. Oda, Y. Hoshi, N. Usami, K. M. Itoh, and S. Tarucha, "A quantum-dot spin qubit with coherence limited by charge noise and fidelity higher than 99.9%," Nat. Nanotechnol. **13**, 102–106 (2018).
[9]P.-A. Mortemousque, E. Chanrion, B. Jadot, H. Flentje, A. Ludwig, A. D. Wieck, M. Urdampilleta, C. Bäuerle, and T. Meunier, "Coherent control of individual electron spins in a two-dimensional quantum dot array," Nat. Nanotechnol. **16**, 296–301 (2021).
[10]C. Volk, A. M. J. Zwerver, U. Mukhopadhyay, P. T. Eendebak, C. J. van Diepen, J. P. Dehollain, T. Hensgens, T. Fujita, C. Reichl, W. Wegscheider, and L. M. K. Vandersypen, "Loading a quantum-dot based 'qubyte' register," npj Quantum Inf. **5**, 1–8 (2019).
[11]A. R. Mills, D. M. Zajac, M. J. Gullans, F. J. Schupp, T. M. Hazard, and J. R. Petta, "Shuttling a single charge across a one-dimensional array of silicon quantum dots," Nat. Commun. **10**, 1063 (2019).
[12]B. Jadot, P.-A. Mortemousque, E. Chanrion, V. Thiney, A. Ludwig, A. D. Wieck, M. Urdampilleta, C. Bäuerle, and T. Meunier, "Distant spin entanglement via fast and coherent electron shuttling," Nat. Nanotechnol. **16**, 570–575 (2021).
[13]H. G. J. Eenink, L. Petit, W. I. L. Lawrie, J. S. Clarke, L. M. K. Vandersypen, and M. Veldhorst, "Tunable coupling and isolation of single electrons in silicon metal-oxide-semiconductor quantum dots," Nano Lett. **19**, 8653–8657 (2019).
[14]B. Bertrand, H. Flentje, S. Takada, M. Yamamoto, S. Tarucha, A. Ludwig, A. D. Wieck, C. Bäuerle, and T. Meunier, "Quantum manipulation of two-electron spin states in isolated double quantum dots," Phys. Rev. Lett. **115**, 096801 (2015).
[15]C. H. Yang, R. C. C. Leon, J. C. C. Hwang, A. Saraiva, T. Tanttu, W. Huang, J. Camirand Lemyre, K. W. Chan, K. Y. Tan, F. E. Hudson, K. M. Itoh, A. Morello, M. Pioro-Ladrière, A. Laucht, and A. S. Dzurak, "Operation of a silicon quantum processor unit cell above one kelvin," Nature **580**, 350–354 (2020).
[16]C. Barthel, D. J. Reilly, C. M. Marcus, M. P. Hanson, and A. C. Gossard, "Rapid single-shot measurement of a singlet-triplet qubit," Phys. Rev. Lett. **103**, 160503 (2009).
[17]A. R. Mills, M. M. Feldman, C. Monical, P. J. Lewis, K. W. Larson, A. M. Mounce, and J. R. Petta, "Computer-automated tuning procedures for semiconductor quantum dot arrays," Appl. Phys. Lett. **115**, 113501 (2019).